Hindawi Publishing Corporation
International Journal of Distributed Sensor Networks
Volume 2012, Article ID 902613, 10 pages
doi:10.1155/2012/902613

Research Article

Experimental Investigation of a Self-Sensing Hybrid GFRP-Concrete Bridge Superstructure with Embedded FBG Sensors

Yanlei Wang, Yunyu Li, Jianghua Ran, and Mingmin Cao

School of Civil Engineering, Dalian University of Technology, Liaoning, Dalian 116024, China

Correspondence should be addressed to Yanlei Wang, wangyanlei@dlut.edu.cn

Received 29 June 2012; Accepted 14 September 2012

Academic Editor: Hong-Nan Li

A self-sensing hybrid GFRP-concrete bridge superstructure, which consists of two bridge decks and each bridge deck is comprised of four GFRP box sections combined with a thin layer of concrete in the compression zone, was developed by using eight embedded FBG sensors in the top and bottom flanges of the four GFRP box sections at midspan section of one bridge deck along longitudinal direction, respectively. The proposed self-sensing hybrid bridge superstructure was tested in 4-point loading to investigate its flexural behavior and verify the operation of the embedded FBG sensors. The longitudinal strains of the hybrid bridge superstructure were recorded using the embedded FBG sensors as well as the surface-bonded electric resistance strain gauges. The experimental results indicate that the embedded FBG sensors can faithfully record the longitudinal strains of the hybrid bridge superstructure in tension at bottom flanges and in compression at top flanges of the four GFRP box sections over the entire loading range, as compared with the surface-bonded strain gauges. So, the proposed self-sensing hybrid GFRP-concrete bridge superstructure can reveal its internal strains in serviceability limit state as well as in strength limit state, and it will have wide applications for long-term monitoring in civil engineering.

1. Introduction

A major concern for many bridge superstructures is the significant reduction in durability and life expectancy caused by the corrosion of the reinforcing steel and the corresponding deterioration of the concrete. These problems are accelerated by the application of deicing salts in cold area. The corrosion will eventually cause enough damage to warrant a superstructure replacement or retrofit [1–3]. It implies that it is imperative to develop and construct bridge systems that have long-term durability and require low maintenance. As one of the solutions to this problem, structural applications of fiber-reinforced polymer (FRP) composites have recently been attractive in the civil engineering community due to their superior material properties such as high corrosion resistance, high specific strength, and high specific stiffness [4]. In spite of all these advantages, FRP composites have higher initial costs and lower stiffness (for glass FRP, GFRP) comparing to conventional materials used in infrastructure applications. To overcome these drawbacks and make the best use of materials, hybrid FRP-concrete structures have been considered as the most effective composite form [5–7].

One of the main reasons preventing greater implementation of FRP composites into the civil infrastructure is the lack of performance data and accepted engineering standards. Using sensors and instrumentation, performance data can be obtained that will provide information on the behavior of the structure over a given time. The integrity of the structure can be established at any phase during the service life of the structure to compensate for other parts of it that are weakening. Smart (or self-sensing) structures will be employed to a greater extent in the future than they are currently [8]. In most designs, crushing of concrete in compression defines the flexural failure of hybrid FRP-concrete bridge superstructure. The failure will be sudden, and hybrid bridge superstructures did not show any ductility [9]. For load bearing elements, the brittle failure is not anticipated because there is no safety prewarning before

the structure failure. So, the monitoring of hybrid FRP-concrete bridge superstructure is essential. Now, structural health monitoring (SHM) has become a hot research topic in the civil engineering. For example, Yi et al. proposed some optimal methods to identify and evaluate civil engineering structure [10–14].

The fiber Bragg grating (FBG) technique is a new technology that proposed important applications in both the telecommunication and the sensing fields [15]. Compared with electric resistance strain gauge, FBG sensor has the advantages of electromagnetic insensitivity, wavelength multiplexing, capability, miniature size, high sensitivity, good long-term stability, and high reliability [16]. FBG sensors can also be easily bonded on the surface of the material or embedded into the structure to measure the strain, temperature, or other physical quantities without affecting the integrity of the structure itself [17].

However, there are some problems in the applications of FBG sensors because the bare FBG sensors are very thin and frangible. They should be packaged or protected before applications. FRP materials lend themselves as prime candidates for the rapidly expanding field of research of "smart (or self-sensing) structures." Smart (or self-sensing) structures are the structures which contain the built-in sensing device to continuously monitor the current state and serviceability of the structures. This is referred to as "passive" smart structures, which have many applications in civil engineering [18, 19]. FRP structures are good candidates for making smart (or self-sensing) structures because their fabrication techniques inherently allow for the embedding of FBG sensors and their communication lines.

In this paper, eight FBG strain sensors will be preembedded in a hybrid GFRP-concrete bridge superstructure during its fabrication process. Embedment of FBG strain sensors in the hybrid GFRP-concrete bridge superstructure leads the bridge superstructure to be a self-sensing bridge superstructure. The flexural behavior of the hybrid bridge superstructure will be investigated, and the monitoring performance of the embedded FBG strain sensors in the hybrid bridge superstructure will also be examined.

2. Proposed Hybrid GFRP-Concrete Bridge Superstructure System

Although many configurations of the hybrid FRP-concrete bridge superstructure are possible, a conceptual design of the hybrid bridge superstructure shown in Figure 1, where supports and substructures are not shown, was chosen. A prototype bridge was designed as a simply supported, single-span, one-lane bridge with a span length of 10 m. Geometric parameters of the cross-section of the bridge in Figure 1(b) were determined to meet the design limit (serviceability check and strength check) by numerous finite-element analyses. The detailed design procedures and finite-element analyses can be found in the literature [20]. The cross-section of the bridge is comprised of 8 GFRP box sections each of which has a layer of concrete in the compression zone.

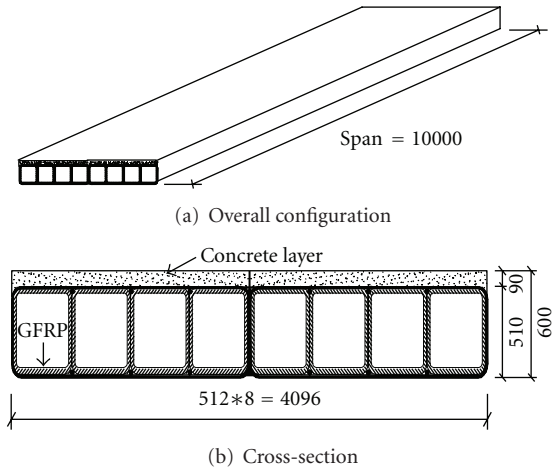

Figure 1: The proposed hybrid bridge superstructure (units in mm).

The bridge design is based on the traditional plank bridge concept, in which a number of individual beams are placed side by side to create a bridge. The advantages of this concept include:

(1) corrosion resistance for steel-free design;

(2) initial costs reduction due to the effective use of concrete;

(3) lightweight;

(4) reduction of local deformation under concentrated loads that is found to be a problem in all-FRP bridge;

(5) no joints between decks and girders (the girders are the decks);

(6) significant understanding of the bridge behavior that can be obtained by testing of individual beams;

(7) the ability to be well understood by bridge engineers.

Four beams make up a bridge deck with a width of 2048 mm. The prototype bridge superstructure consists of two bridge decks. The 2048 mm wide bridge deck can be easily transported to site on a standard truck and assembled into a bridge using simple field joints.

3. Experimental Program

3.1. Specimen Preparation. The test specimen (described in Figure 2) is a one-third scale model of the 10 m hybrid GFRP-concrete bridge superstructure shown in Figure 1. As previously mentioned, the hybrid bridge superstructure consists of two individual hybrid bridge decks (shown in Figure 2(a)). The geometry of cross-section and the locations of the embedded FBG sensors (FBG) and surface-bonded electric resistance strain gauges (SGs) of one hybrid GFRP-concrete bridge deck (test specimen) are shown in Figure 3. Eight FBG sensors were designed to be embedded into the top and bottom flanges of the GFRP part at midspan section of one bridge deck along the longitudinal direction,

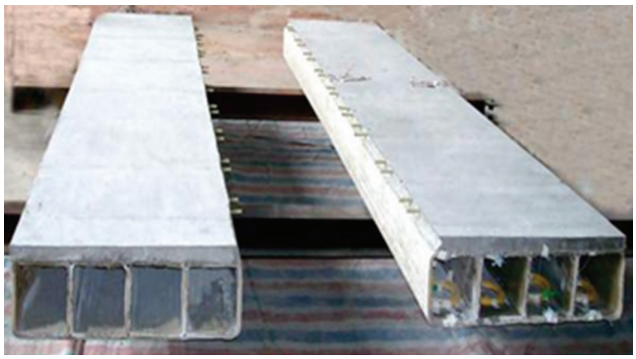

(a) Two individual bridge decks

(b) Bridge superstructure

Figure 2: The photographs of the test specimen.

respectively, to form the self-sensing hybrid GFRP-concrete bridge superstructure. The embedded FBG sensors were used to monitor the internal compressive and tensile strains of the bridge superstructure, respectively.

As a trial test, the GFRP part of the test specimen was fabricated by hand lay-up process at present. Two types of stitched bidirectional E-glass fabric with a weight of 600 g/m^2, (0°/90°), and (±45°) were selected as the primary continuous reinforcement in this study. In these fabrics, fibers in 0° and 90° or +45° and −45° directions have the same weight (300 g/m^2), respectively. Vinyl ester resin, Swancor 901, was selected as the matrix for the GFRP part. The vinyl ester resin was selected because of its high flexibility and impact resistance, its lower cost compared to other resin systems, and its good performance in harsh filed environments. Therefore, it is very suitable for civil engineering structures.

The fabrication process of the proposed self-sensing hybrid GFRP-concrete bridge superstructure is as follows.

Firstly, eight individual GFRP box beams were fabricated. The top flange and two webs of each GFRP box section had the same fiber architecture, which consisted of 12 layers of woven fabric reinforcement. However, the bottom flange of the GFRP box section consisted of 18 layers of woven fabric to increase the global stiffness of the section. Stacking sequences of the top and bottom flanges were $[(90°/0°)_3, (\pm45°)_2, (0°/90°)]_s$ and $[(90°/0°)_3, (0°/90°)_3, (\pm45°)_2, (0°/90°)]_s$, respectively.

Secondly, by combining two sets of four box beams each using vinyl ester resin and chopped strand mat (CSM), two sections with a width of approximately 680 mm were created.

Thirdly, the two sections were wrapped individually with a $[(90°/0°)_2]_s$ outer laminate (shown in Figure 3) to strengthen the transverse stiffness of the sections of the bridge deck. Eight FBG sensors were designed to be embedded into the outer laminate at the top and bottom flanges of GFRP part at midspan section of one bridge deck along the longitudinal direction (shown in Figure 3(b)), respectively. FBG sensors were located at the middle location of the top and bottom flanges of each GFRP box section. Eight electric resistance strain gauges were attached on the surface of GFRP part where FBG sensors were embedded (shown in Figure 3(b)) to investigate the strain sensing properties of the embedded FBG sensors. Stacking sequences of the outer laminate with FBG sensor were $[(90°/0°)_2, \{\text{FBG-}0°\}, (0°/90°)_2]$. It has also been widely documented that for optimum transfer of strain from host material to sensor, the sensor should be aligned parallel to the reinforcing fiber [21]. When sensors were embedded parallel to the direction of reinforcing fiber, resin-rich areas around the sensor gage were prevented. It was assumed that this placement minimized nonuniform stress fields around the sensor, which could reduce measurement accuracy [22]. Stitching/bonding FBG sensors to the fabric reinforcement was the least invasive method to prevent sensor slippages (shown in Figure 4).

Fourthly, concrete was cast on the top surfaces of the two sections, respectively, forming the scaled hybrid GFRP-concrete bridge decks (shown in Figure 2(a)). To develop a good bond between GFRP part and concrete, 5∼10 mm aggregate was applied to the top flange of GFRP part with epoxy adhesive. Applying too much or too little aggregate could create insufficient bond between GFRP and concrete for the two materials to act compositely. The aggregate distribution percentage was recommended to be 35% ∼45% to obtain the optimal bond [23].

Finally, the two bridge decks were assembled together by a simple method (shown in Figure 5), forming the proposed scaled hybrid GFRP-concrete bridge superstructure (shown in Figure 2(b)).

As previously mentioned, the FBG sensors were embedded into FRP parts. So, the embedded FBG sensors could suit for the extensive civil engineering construction without any protective measure. However, the outside optical fiber wire needs additional protective measure. Usually, the Kevlar fiber optic wire was used as a protective measure to ensure its optimal performance and avoid being broken.

The fiber volume fraction of the GFRP part is about 0.3. The material properties of the GFRP part are recorded in Table 1. Due to the size of the test specimen, coarse aggregates with maximum size of 10 mm were used in the concrete. The compressive strength of the concrete on the day of test is 51 MPa from 150 mm × 150 mm × 150 mm concrete cube. According to the Chinese concrete code (GB 50010-2010), Young's modulus of the concrete of 36.46 GPa is obtained by theoretical calculation with the concrete strength of 51 MPa. However, the true Young's modulus of

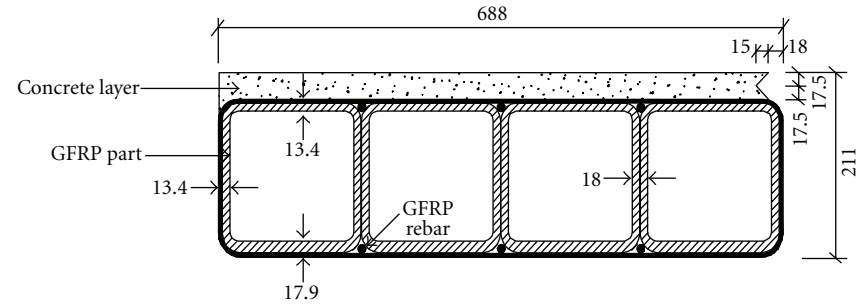

(a) Geometry of cross-section of one bridge deck

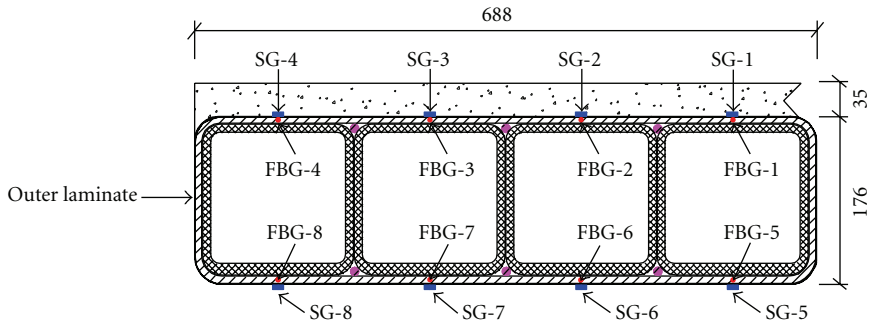

(b) Locations of FBG sensors and strain gauges (SG) in one bridge deck

Figure 3: The proposed self-sensing hybrid GFRP-concrete bridge deck (units in mm).

Table 1: Material properties of GFRP part.

Type of material test	Module of elasticity/GPa	Poisson ratio	Strength/MPa
Longitudinal tension of bottom flange	15.14	0.18	245
Longitudinal tension of top flange and outer web	14.44	0.19	240
Longitudinal tension of inner web	14.05	0.21	237
In-plane shear of outer web	3.36	—	120
In-plane shear of inner web	3.69	—	120

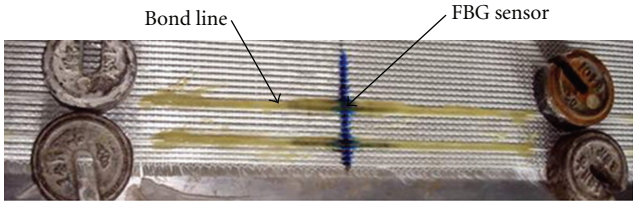

Figure 4: Bonding FBG sensors to the fabric reinforcement.

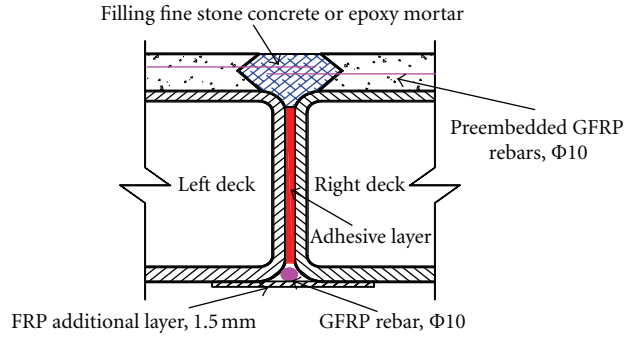

Figure 5: Connecting details between two hybrid bridge decks.

the concrete will be slightly smaller than the normal concrete due to the use of small size coarse aggregates.

3.2. Strain Calibration. The strain sensitivity coefficient of FBG sensors will be different because of the different fiber, writing, annealing, and packaging techniques for FBG sensors. So, the strain sensitivity coefficients of the embedded FBG sensors into GFRP should be determined through strain calibration experiments before their applications.

According to ASTM D3039 standard test procedures, two test specimens with embedded FBG sensors were fabricated and cut from two laminates. Stacking sequences of the two laminates were the same as those of the top and bottom flanges of the GFRP part mentioned in Figure 3, respectively. The dimensions and schematic view of specimen are shown in Figure 6. Aluminum tabs were attached on the specimen to prevent damage of the leads from gripping pressure during the uniaxial tensile test. Before testing, two electrical

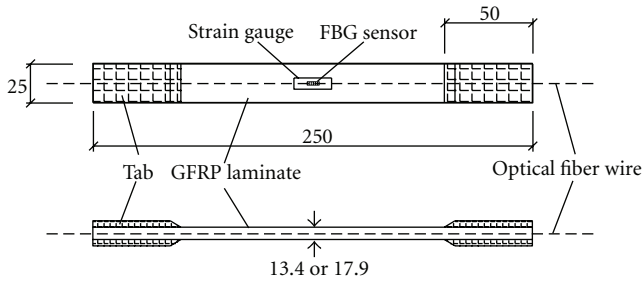

Figure 6: Schematic illustration showing the relative positions of FBG sensor and strain gauges and specimen dimension (units in mm).

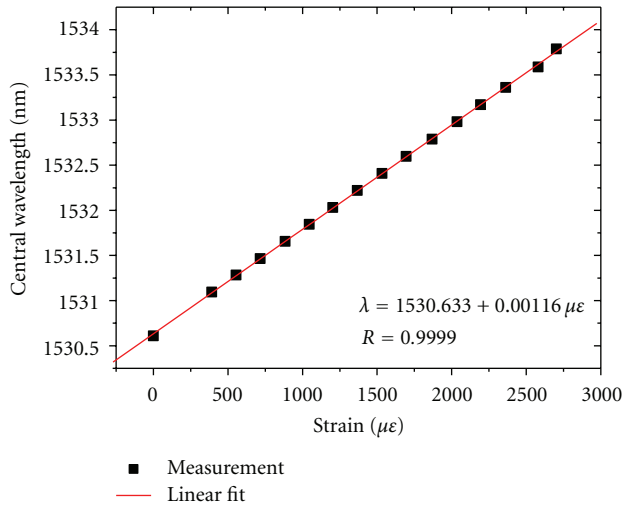

Figure 7: Relationship between FBG's wavelength and strain for the specimen from top flange.

strain gauges were bonded side by side on the surface of each specimen where FBG sensor was embedded (shown in Figure 6). The test was conducted on a universal material experimental machine. The FBG interrogation system was provided by MOI Ltd. with model number si-720. In this test, the effect of temperature changes was not considered due to the fact that the experiment was conducted in the laboratory in a short time.

The results of the calibration test are shown in Figures 7 and 8. The strain sensing coefficients of the two test specimens are 1.16 pm/$\mu\varepsilon$ and 1.17 pm/$\mu\varepsilon$ for the top flange and bottom flange of the hybrid bridge superstructure, respectively, which correlate well with that of bare FBG sensors whose value is about 1.2 pm/$\mu\varepsilon$. Based on the precision of si-720 interrogation system, the strain sensing precision of the specimens is near 1 $\mu\varepsilon$. From the two figures, we can see that the shifts of center wavelength of FBG sensors are in a good linear relationship with the strains measured by the strain gauges. And the linear correlation coefficients of the two specimens all reach 0.9999.

3.3. Test Setup and Loading Protocols. The test setup is shown in Figure 9. Loads were applied vertically at four points on

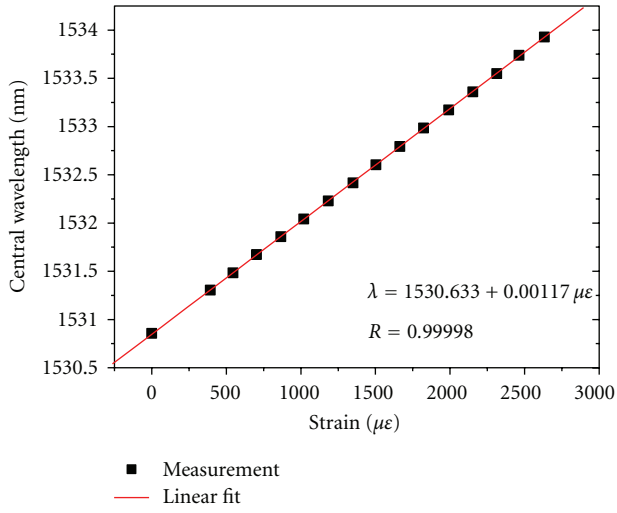

Figure 8: Relationship between FBG's wavelength and strain for the specimen from bottom flange.

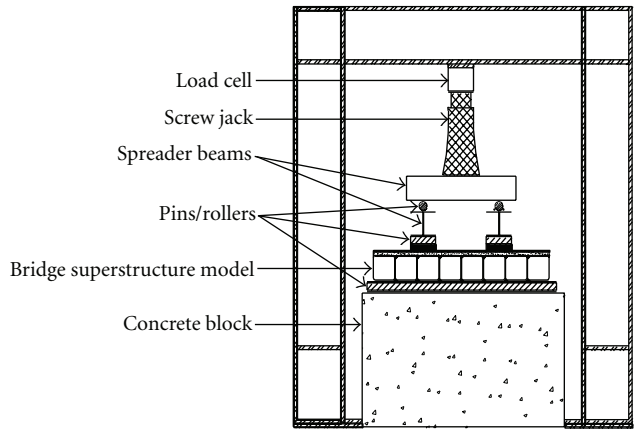

Figure 9: Experimental setup.

the top surface of the test specimen by three spreader beams and the screw jack supported by the top beam of a reaction frame. The load configuration simulates the two heaviest axles of the standard truck load (total 5 axles) specified in the Chinese bridge design specifications (JTG D6-2004). In the specifications, the design truck load is a live load and has 5 axles. And the two heaviest axles are specified as 140 kN each, where one axle is 1.4 m away from the other. Each axle has two tires that are 1.8 m apart center-to-center, and each tire area has a length of 0.6 m and a width of 0.2 m. For the 1/3 scale model, this design truck load becomes two axles of 31.12 kN, 0.467 m apart. Two tires of axle are 0.6 m apart, and each tire area is 0.2 m long and 0.067 m wide. The test specimen was simply supported on rollers with a span length of 3333 mm and a support length of 0.2 m at each end. The loading configuration of the flexural test is shown in Figure 10. To protect the bottom surface of the specimen from damage, rubber pads were placed between test specimen and the pin/roller at two ends of the specimen.

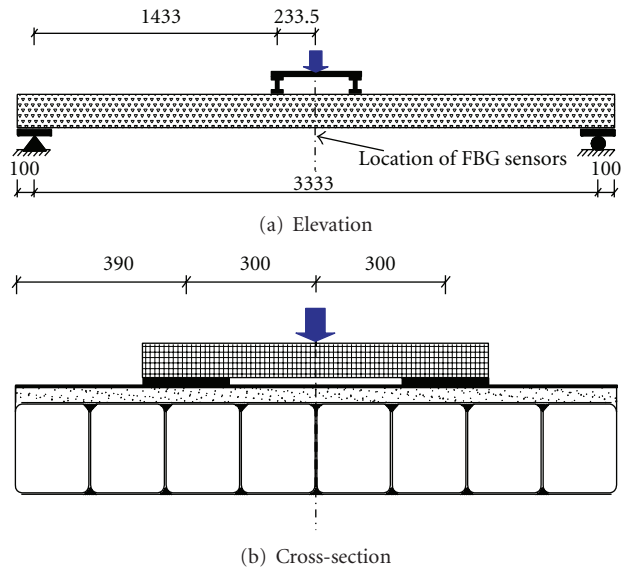

Figure 10: Loading configuration of the hybrid bridge superstructure.

As mentioned in Section 3.1, eight FBG sensors were embedded into the midspan section of one hybrid GFRP-concrete bridge deck. Eight surface-bonded electrical resistance strain gauges (shown in Figure 3(b)) were also used to check the accuracy of the output of the embedded FBG sensors. A four-point loading test was conducted to investigate the flexural behavior and the strain response measured from FBG sensors for the proposed self-sensing hybrid GFRP-concrete bridge superstructure. The strain sensing performances of the embedded FBG sensors were recorded by the Micron Optical Sensing Interrogator (MOI Ltd., si-720). And the data of the electric resistance strain gauges were gathered using the Static Strain Acquisition Device (DongHua Test Inc.). In this test, the change of temperature was not considered to simplify the analysis because the test time was short, the temperature of the laboratory almost did not change during the test, and the monitoring values were large (the maximum value was 0.857%, stated in Section 4.2). However, there will be large temperature variation in field application. Due to the fact that FBG senses both strain and temperature simultaneously, temperature compensation for FBG strain sensors of long-term field monitoring system is indispensable. And many solutions to temperature compensation have been developed [24].

The flexural test was performed by force control, and it was divided into two steps: Step I and Step II, shown in Figure 11, in order to evaluate its performance and meet the objectives of the research. In the first step (Step I), force history of a triangular shape with the load amplitude gradually increased was applied to examine the deflection stabilization. In the second step (Step II), force had been increased monotonically until the test specimen failed. In Figure 11, as previously mentioned, "Truck Load" is two axles load of 31.12 kN.

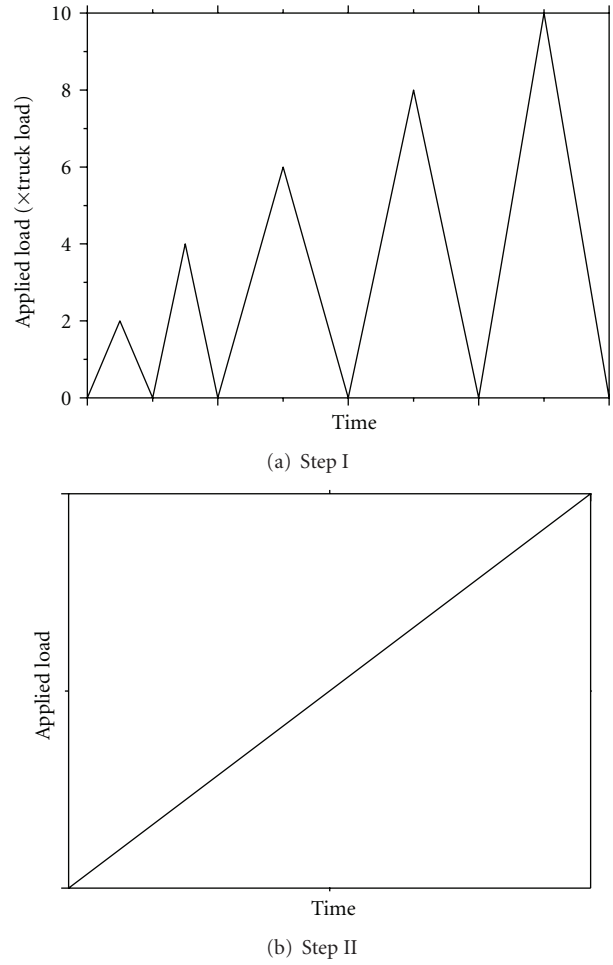

Figure 11: Loading protocols of the test.

4. Test Results and Discussions

4.1. Load-Deflection Response and Failure Mode. Figure 12 shows load-deflection responses obtained at central point of midspan section of the test specimen during Step I and Step II. No sound of cracking of either the concrete or GFRP was heard during Step I. Visual inspection after the test revealed no cracking in the surface of the test specimen. It can be concluded that the obtained load-deflection response is very much linear and has a good repeatability for the hybrid bridge specimen during Step I.

At the load of near 16 × truck load in Step II, there was a medium loud noise. It is regretted that visual inspection was not conducted in time. So, the noise may be caused by the cracking of the interface between GFRP and concrete or the cracking of concrete under the loading points. And at this point, the slope of load-deflection curve changes slightly. The load was 8.8 times the Chinese bridge design requirement of 1.4(1 + IM) × truck load for live loads in the strength limit state, where IM = dynamic load allowance, and has a value of 0.3 in this case. Since the dead load and other live loads were not considered appropriately in this test, 8.8 cannot be called the safety factor.

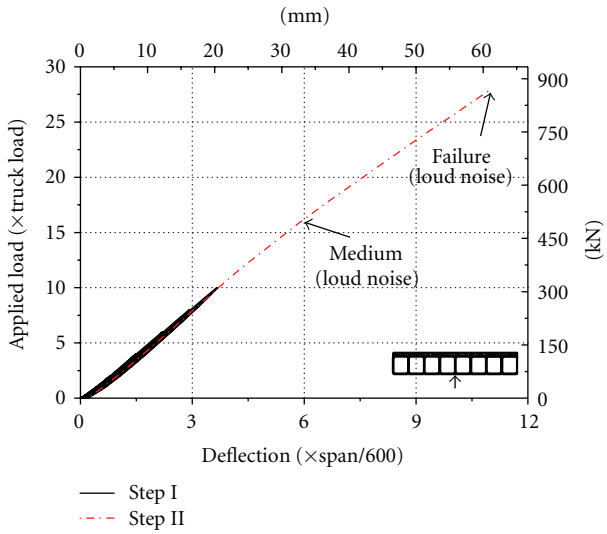

FIGURE 12: Load versus deflection at central point of midspan section.

Figure 12 shows that the loading path is nearly linear until the specimen failed. A global failure as shown in Figure 13 occurred at 28 × truck load, which is 15.4 times the 1.4(1 + IM) × truck load. Crushing of concrete in compression near the loading points defines flexural collapse of test specimen. However, the GFRP part was found to be intact. This can be described as follows. As concrete failed, large deflection occurred immediately due to the low stiffness of GFRP part in comparison to the hybrid section, along with instantaneous reduction of the load for the quick increase of deflection, and the combined compression capacity of the GFRP top flange and the residual strength of the concrete enable the specimen to carry the residual load. After unloading the residual load, the deflection of the specimen almost came back. The failure was sudden due to the nature of the concrete. However, the obtained failure mode is considered to be favorable because it did not lead to collapse of the entire bridge, and the bridge can be retrofitted easily by the replacement of the concrete layer.

As pointed out by the Chinese road authorities, trucks in excess of many times the legal limit have been detected in China. These extreme loads can initiate cracks or cause damage in a bridge structure, which may propagate under subsequent dynamic load, resulting in a significantly decreased life span. However, the proposed bridge model has significant reserve strength. It will be of great benefit for the ubiquity of overload operation in China.

There was no visual failure in the connection between GFRP and concrete before the failure of the bridge superstructure. This phenomenon reflects that using aggregate coating is an efficient method to ensure composite action between GFRP and concrete for the proposed hybrid bridge superstructure.

4.2. Self-Sensing Performance. The locations of the embedded FBG sensors and surface-bond strain gauges in the proposed self-sensing hybrid bridge superstructure are illustrated in Figure 3(b). Strains from eight FBG sensors

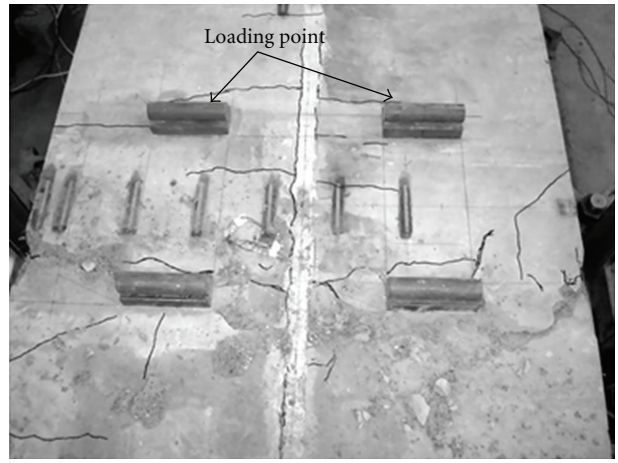

(a) Top view

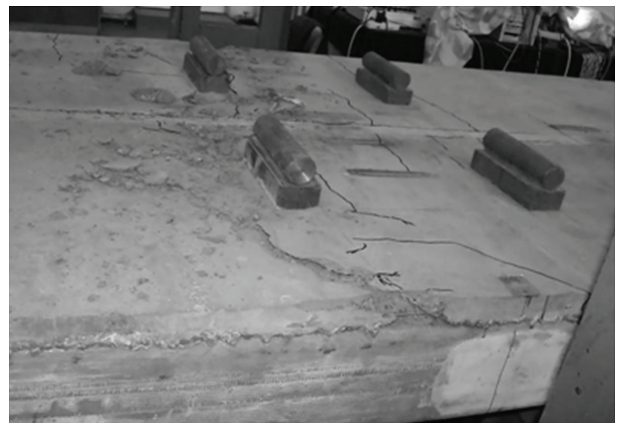

(b) Side view

FIGURE 13: Failure of test specimen.

and eight strain gauges of the self-sensing hybrid bridge superstructure during Step I are shown in Figure 14. Strains from FBG sensors are obtained based on the strain sensing coefficients calibrated in Section 3.2. This figure shows that there is a good agreement between FBG sensor and strain gauge in tensile status at bottom flange of the GFRP part, as well as in compressive status at top flange of the GFRP part. And we can see that the repeatability and consistency of the embedded FBG sensors and surface-bond strain gauges are remarkable. From Figure 14, we can find that the outputs of FBG sensors are slightly smaller than those of strain gauges. The reason is that the locations of them are different in the cross-section of the self-sensing hybrid bridge superstructure (shown in Figure 3(b)). So, the outputs of them should be slightly different based on the assumption of plane section.

Figure 15 shows the measured strains from eight FBG sensors and eight strain gauges in the self-sensing hybrid bridge superstructure during Step II. There is an excellent agreement between the eight FBG sensors and the eight strain gauges in tensile and compressive status over the entire load range, respectively. Because of the same reason previously mentioned, the outputs of FBG sensors are slightly smaller than those of strain gauges. And the maximum tensile and

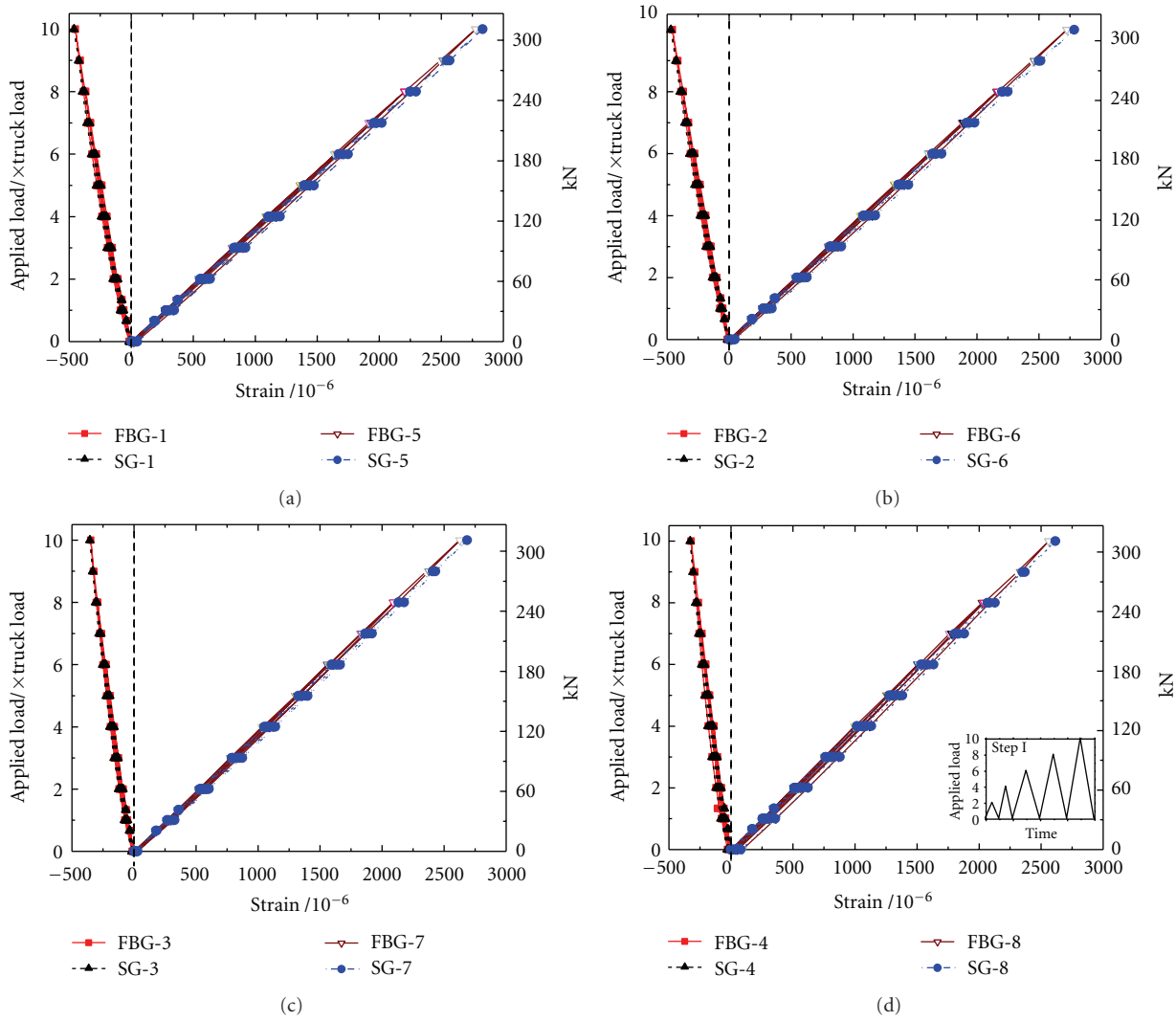

Figure 14: Strains from eight FBG sensors and eight strain gauges in the self-sensing hybrid bridge superstructure during Step I.

compressive strains recorded by the embedded FBG sensors are 0.857% (from FBG-5) and −0.186% (from FBG-1) at failure of the self-sensing hybrid bridge superstructure, respectively.

We can conclude that the embedded FBG sensors can monitor the internal strain of the proposed self-sensing hybrid GFRP-concrete bridge superstructure over the entire load range from zero to the failure of the bridge superstructure. It indicates that the embedded FBG sensors can monitor the internal strain of the composite bridge superstructure in normal service state as well as in limit state.

5. Conclusions

A self-sensing hybrid GFRP-concrete bridge superstructure was developed by embedding eight FBG sensors into GFRP part to monitor the internal longitudinal strains of the proposed hybrid bridge superstructure. Experiment for strain calibration of the GFRP laminates with embedded FBG sensors was conducted firstly on material test system, and the strain sensing property of the laminates is nearly the same as that of bare FBG sensors. Then, a 4-point loading test was carried out to assess the flexural behavior of the proposed self-sensing hybrid GFRP-concrete bridge superstructure and the feasibility of strain monitoring of the embedded FBG sensors. Compared with the surface-bonded electric resistance strain gauges, the FBG sensors can faithfully record the longitudinal internal strain of the hybrid bridge superstructure in tension and in compression over the entire load range. It indicates that the embedded FBG sensors can monitor the internal strain of the hybrid GFRP-concrete bridge superstructure in serviceability limit state as well as in strength limit state. The proposed self-sensing hybrid GFRP-concrete bridge superstructure has a good capability of monitoring its internal strain in its service life and is very suitable for the long-term monitoring.

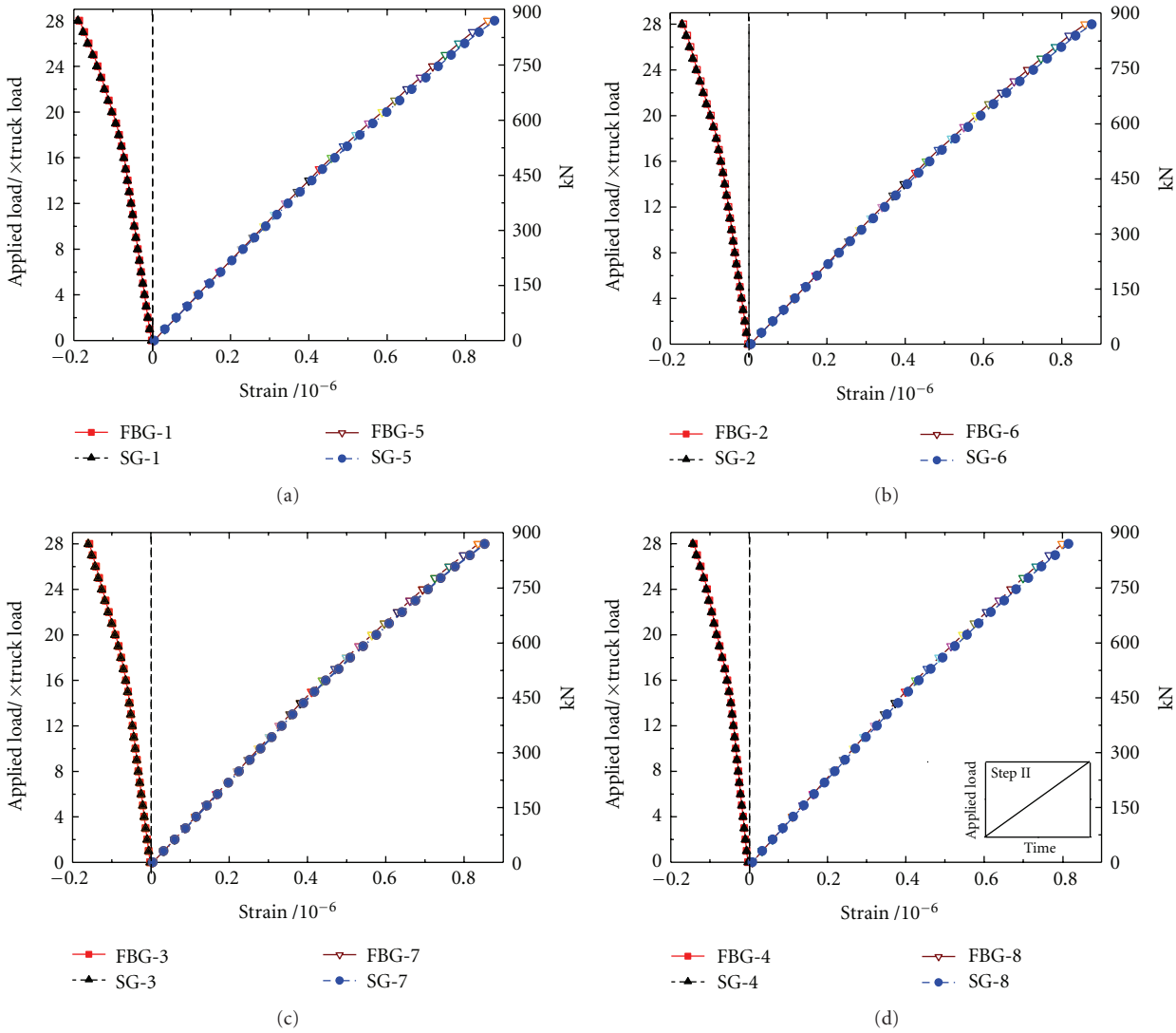

Figure 15: Strains from eight FBG sensors and eight strain gauges in the self-sensing hybrid bridge superstructure during Step II.

Acknowledgments

The authors gratefully acknowledge the financial support provided by the National Key Basic Research Program of China (Project no. 2012CB026203), the Natural Science Foundation of China (Project no. 50908030), the National Key Technologies R&D Program of China (Project no. 2011BAK02B03), and China Postdoctoral Science Foundation (Project no. 201003620).

References

[1] W. Alnahhal and A. Aref, "Structural performance of hybrid fiber reinforced polymer-concrete bridge superstructure systems," *Composite Structures*, vol. 84, no. 4, pp. 319–336, 2008.

[2] L. Cheng and V. M. Karbhari, "New bridge systems using FRP composites and concrete: a state-of-the-art review," *Progress in Structural Engineering and Materials*, vol. 8, no. 4, pp. 143–154, 2006.

[3] L. Van Den Einde, L. Zhao, and F. Seible, "Use of FRP composites in civil structural applications," *Construction and Building Materials*, vol. 17, no. 6-7, pp. 389–403, 2003.

[4] Y. Kitane, A. J. Aref, and G. C. Lee, "Static and fatigue testing of hybrid fiber-reinforced polymer-concrete bridge superstructure," *Journal of Composites for Construction*, vol. 8, no. 2, pp. 182–190, 2004.

[5] A. Mirmiran, "Innovative combinations of FRP and traditional materials," in *Proceedings of the International Conference on FRP Composites in Civil Engineering*, pp. 1289–1298, Elsevier Science, Hong Kong, China, 2001.

[6] G. P. Warn and A. J. Aref, "Sustained-load and fatigue performance of a hybrid FRP-concrete bridge deck system," *Journal of Composites for Construction*, vol. 14, no. 6, pp. 856–864, 2010.

[7] T. Keller, E. Schaumann, and T. Vallée, "Flexural behavior of a hybrid FRP and lightweight concrete sandwich bridge deck," *Composites Part A*, vol. 38, no. 3, pp. 879–889, 2007.

[8] L. C. Hollaway, "The evolution of and the way forward for advanced polymer composites in the civil infrastructure,"

Construction and Building Materials, vol. 17, no. 6-7, pp. 365–378, 2003.

[9] Y. Wang, Q. Hao, and J. Ou, "Flexural testing of fiber reinforced polymer-concrete composite bridge superstructure," *Advanced Materials Research*, vol. 79–82, pp. 1855–1858, 2009.

[10] T. H. Yi, H. N. Li, and M. Gu, "A new method for optimal selection of sensor location on a high-rise building using simplified finite element model," *Structural Engineering and Mechanics*, vol. 37, no. 6, pp. 671–684, 2011.

[11] T. H. Yi, H. N. Li, and M. Gu, "Characterization and extraction of global positioning system multipath signals using an improved particle-filtering algorithm," *Measurement Science and Technology*, vol. 22, no. 7, Article ID 075101, pp. 1–11, 2011.

[12] T. H. Yi, H. N. Li, and M. Gu, "Optimal sensor placement for structural health monitoring based on multiple optimization strategies," *The Structural Design of Tall and Special Buildings*, vol. 20, no. 7, pp. 881–900, 2011.

[13] T. H. Yi and H. N. Li, "Methodology developments in sensor placement for health monitoring of civil infrastructures," *International Journal of Distributed Sensor Networks*, vol. 2012, Article ID 612726, 11 pages, 2012.

[14] T. H. Yi, H. N. Li, and X. D. Zhang, "A modified monkey algorithm for optimal sensor placement in structural health monitoring," *Smart Materials and Structure*, vol. 21, no. 10, Article ID 05033, pp. 1–9, 2012.

[15] R. J. Sun, Z. Sun, D. H. Dan, and L. M. Sun, "An integrated FBG sensing system for bridge health monitoring," in *Smart Structures and Materials 2006—Sensors and Smart Structures Technologies for Civil, Mechanical, and Aerospace Systems*, vol. 6174 of *Proceedings of SPIE*, pp. 1–7, 2006.

[16] Y. L. Wang, Q. D. Hao, and J. P. Ou, "Experimental testing of a self-sensing FRP-concrete composite beam using FBG Sensors," in *Sensors and Smart Structures Technologies for Civil, Mechanical, and Aerospace Systems*, vol. 7292 of *Proceedings of SPIE*, pp. 1–9, 2009.

[17] Y. L. Wang, Z. Zhou, and J. P. Ou, "Study on fabrication of smart FRP-OFBG composite laminates and their sensing properties," in *Fundamental Problems of Optoelectronics and Microelectronics III*, vol. 6595 of *Proceedings of SPIE*, pp. 1–6, 2007.

[18] A. L. Kalamkarov, S. B. Fitzgerald, D. O. MacDonald, and A. V. Georgiades, "Smart pultruded composite reinforcements incorporating fiber optical sensors," in *Structural Materials Technology III*, vol. 3400 of *Proceedings of SPIE*, pp. 94–105, 1994.

[19] J. P. Ou, Z. Zhou, Z. J. Wu, S. Z. Tian, and X. F. Zhao, "Optical FBGs' sensing properties and practical application in civil infrastructures," in *Fundamental Problems of Optoelectronics and Microelectronics*, vol. 5129 of *Proceedings of SPIE*, pp. 10–17, 2003.

[20] Y. L. Wang, *Experimental investigation, analytical and design methods for hybrid FRP-concrete beam/bridge superstructure systems [Ph.D. dissertation]*, Harbin Institute of Technology, Harbin, China, 2008.

[21] S. Moloney, M. J. Connelly, and P. A. Butler, "Strain sensing in carbon composite material using embedded fibre Bragg grating sensors," in *Opto-Ireland 2005: Optical Sensing and Spectroscopy*, vol. 5826 of *Proceedings of SPIE*, pp. 645–653, 2005.

[22] R. Lopez-Anido and S. Fifield, "Experimental methodology for embedding fiber optic strain sensors in fiber reinforced composites fabricated by the VARTM/SCRIMP process," in *Proceedings of the 4th International Workshop on Structural Health Monitoring*, pp. 247–254, 2003.

[23] A. C. Berg, *Analysis of a bridge deck built on U.S. highway 151 with FRP stay-in-place forms, FRP grids, and FRP rebars [M.S. thesis]*, University of Wisconsin-Madison, Madison, Wis, USA, 2004.

[24] Z. Zhou and J. P. Ou, "Techniques of temperature compensation for FBG strain sensors used in long-term structural monitoring," in *Fundamental Problems of Optoelectronics and Microelectronics II*, vol. 5851 of *Proceedings of SPIE*, pp. 167–172, 2005.